

---

# Stability and dewetting of thin liquid films

Karin Jacobs,<sup>1</sup> Ralf Seemann,<sup>1,2</sup> and Stephan Herminghaus<sup>2</sup>

<sup>1</sup> Dept. of Experimental Physics, Saarland University, D-66123 Saarbrücken, Germany.

<sup>2</sup> Max-Planck-Institute for Dynamics and Self-Organization, D-37073 Göttingen, Germany.

**Summary.** The stability of thin liquid coatings is of fundamental interest in everyday life. Homogeneous and non-volatile liquid coatings may dewet either by heterogeneous nucleation, thermal nucleation, or spinodal dewetting. Wetting and dewetting is explained on a fundamental level, including a discussion of relevant interactions. The chapter will also address the various dewetting scenarios and explain how the effective interface potential governs the behavior obtained for various stratified substrates and film thicknesses.

## 1 Introduction

'To wet or not to wet' [1] is the question this chapter tries to answer. It concerns the fundamental aspects of the stability of thin liquid films or coatings. The liquid in question can be any homogeneous liquid<sup>3</sup>, such as, e.g., an aqueous solution, an oil, or a polymer melt. Whether or not a liquid wets a given surface is not only of fundamental interest, but also of substantial technical importance. The authors have been approached by numerous companies with interesting problems concerning wettability, ranging from the automotive industry, the pharmaceutical and chemical industry, to the food processing, printing, and textile industry. In principle, the general answer to all wettability problems is simple: a liquid wets a surface if it can gain energy by enlarging the interface with that substrate. To provide this answer for a specific system under study, however, may be quite cumbersome. Below we provide what may be seen as a map to reader to help with a first encounter with thin liquid film stability problems. For the sake of clarity, we restrict our considerations to liquids on solid, homogeneous substrates.

---

<sup>3</sup> homogeneous on the length scale set by the thickness of the liquid film under consideration. In particular, demixing or segregation effects are thereby assumed to be negligible.

## 2 Experimental model systems for simple liquids

In order to study the basic mechanisms of a certain class of phenomena, it is of central importance to identify suitable model systems. Since the main problems in the controlled preparation of thin films and surfaces lies in their inherent propensity to become contaminated by dust or other impurities, the first quantitative studies of surface forces in wetting films have been performed with cryogenic systems, in which impurities are naturally frozen out [2, 3, 4]. However, it has been realized that these systems involve strong exchange of material between the liquid and vapor phase and thus are not well suited for studies of dynamic aspects, such as dewetting and structure formation phenomena.

Thin laser-annealed metal films were candidates,[5, 6] yet the same time, techniques of preparing systems which involve more complex liquids, such as polymer melts, in a well-defined and clean way became progressively available. As a result, the numerous benchmark studies of the basic mechanisms of dewetting have been performed with polymer melts (see e.g. the review articles of D.G. Bucknall[7] and P. Müller-Buschbaum[8]). Systematic experimental studies were begun somewhere around the 1990s [9, 10, 11, 12, 13] inspired by P.-G. de Gennes' theoretical work.[15, 14] Polymer melts are on the one hand close to application (coatings, photo resist), yet on the other hand easily controllable in the experiments. Polymers such as polystyrene (PS) are very suitable model liquids since they have a very low vapor pressure in the melt, and mass conservation can safely be assumed. Moreover, they are chemically inert, non-polar, and their dynamics can be tailored by choosing different chain lengths and annealing temperatures. For molecular weights below the entanglement length ( $\sim 17$  kg/mol), the melt can safely be treated as simple (Newtonian) liquid for the low shear rates in dewetting experiments[16, 17]. Below the glass transition temperature  $T_g$ , the films are glassy and can be stored for subsequent analysis<sup>4</sup>. PS in atactic steric configuration moreover does not exhibit any tendency for crystallization.

As substrates, typically hydrophobized Si wafers with their natural amorphous Si dioxide layer (SiO<sub>2</sub>) have been widely used. the present chapter thus concentrates on Si wafers as substrates, which can be purchased with a very small surface roughness (rms roughness smaller than 0.2 nm). The wettability of these substrates can be tuned by chemically grafting monomolecular functional layers onto the native silicon oxide overlayer. For instance, hydrophobization is often achieved by grafting a self-assembled monolayer of octadecyl-trichlorosilane[25, 26] onto the wafer.

For dewetting experiments it is necessary to prepare a thin liquid film in a non-equilibrium state on a substrate. Usually, a thin polymer coating is prepared from a solvent solution by one of the following standard techniques:

---

<sup>4</sup> It is important to note that  $T_g$  of thin films can be substantially different (mostly lower) than the bulk value.[18, 19, 20, 21, 22, 23, 24]

spin coating, dip coating, or spraying<sup>5</sup>. The solvent evaporates during the preparation procedure, leaving behind a smooth, glassy polymer layer. By spin coating a solution of polystyrene in toluene one can easily achieve a PS layer of thickness in the range of a few nanometers up to several micrometers. The roughness of the polystyrene layer is then similar to the underlying substrate. For experimental details and caveats of preparation, the reader is referred to the pertinent literature. [27, 13, 28, 10, 29, 16, 30] The thickness of the films can be determined by standard techniques, such as ellipsometry[31]. The dewetting process can be studied by optical microscopy and/or atomic force microscopy (AFM). Most studies use AFM in non-contact mode operation to avoid any damage of the soft surface, which even allows to image the dewetting scenario in situ[32, 33].

To induce dewetting, the films are heated above the glass transition temperature. Figure 1 shows a series of optical micrographs of an 80 nm thick PS film of molecular weight of 65 kg/mol ('PS(65k)') dewetting a silanized Si wafer. The series depicts a pattern formation process that is typical for most dewetting films, whether for a water film on a waxed surface, or a coating on a dusty substrate.

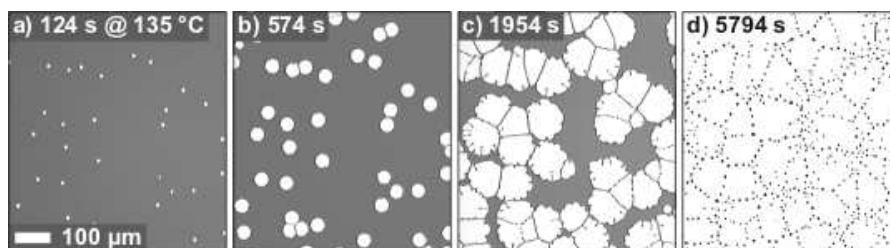


**Fig. 1.** Pictures series taken by a light microscope: a 80 nm thick polystyrene film of 65 kg/mol molecular weight is dewetting at 135°C from a hydrophobized silicon substrate for approximately (from left to right) 2 min, 10 min, 30 min, and 100 min.

The process of dewetting can be divided into three stages: in the early stage, holes are generated by a rupture process, c.f. Fig. 1a; in the intermediate stage, the radius of the holes increases, leading to hole coalescence, c.f. Fig. 1b-c. In the intermediate stage, the focus is on the dynamics involved in the dewetting process, its impact on the hole profiles and on its influence on dewetting patterns. From the dynamics of hole growth [27, 36, 34, 35, 37, 28, 38, 39, 40] as well as from the shape of the liquid rim surrounding the hole one can get information about the slip or no-slip boundary condition of the liquid close to the solid substrate [17, 41, 42]. In the late stage, the straight

<sup>5</sup> For all these techniques, the surface to be coated must be wettable by the polymer solution. Otherwise, the film must be prepared on another substrate, e.g. mica, and then transferred to the surface of interest.

ribbons that separate two coalescing holes decay into droplets due to the Rayleigh-Plateau instability[43], c.f. Fig. 1c-d. Slight differences in the size of the droplets cause slight pressure differences, leading small droplets to shrink and large droplets to grow (Ostwald ripening[44]). Due to the small vapor pressure and the low mobility of the polymer molecules, the ripening process is extremely slow. Most experiments are stopped before the 'final state', i.e. one single drop on the surface, is reached. In what follows, we focus on the initial stage of dewetting: why does the polystyrene film dewet the hydrophobized Si wafer at all? The next section will be dedicated to the discussion of the various energy contributions involved, and their mutual balance.

### 3 The energy balance

In a Teflon<sup>®</sup> coated frying pan a stable oil layer can only be achieved if one pours enough oil into the pan. Gravity then stabilizes the thick oil film. If the oil film thins well below the so-called capillary length  $\lambda_{cap}$ , capillary (intermolecular) forces dominate over gravitational forces and the film may dewet [45]. The capillary length is given by  $\lambda_{cap} = \sqrt{\sigma_{lv}/\rho g}$  (for olive oil:  $\lambda_{cap} \approx 1.7$  mm, for water:  $\lambda_{cap} \approx 2.7$  mm), where  $\sigma_{lv}$  is the liquid/vapor surface tension and  $\rho$  the density of the liquid. Therefore, dewetting of liquid films driven by intermolecular forces can only occur for 'thin' films, i.e. films thinner than  $\lambda_{cap}$ .

A liquid can be metastable and then needs a nucleus to induce dewetting. In the following we will focus on liquid films thinner than  $\lambda_{cap}$  and discuss under which conditions a thin liquid layer will be stable, metastable or unstable on top of a substrate.

#### 3.1 The Young equation

Dewetting is a dynamic process that begins in a non-equilibrium situation [46, 47, 48, 49, 50, 14, 51, 52], namely the flat film on the surface and ends when reaching an equilibrium state, one droplet or a set of droplets<sup>6</sup>. Thus, let us first start with a droplet, c.f. Fig. 2:

A droplet on a homogeneous surface usually exhibits the form of a spherical cap and the tangent to the droplet at the three phase contact line includes an angle  $\theta$  with the substrate. In equilibrium, the angle is given by a balance of macroscopic forces:

$$\cos \theta = \frac{\sigma_{sv} - \sigma_{sl}}{\sigma_{lv}} \quad (1)$$

This is the Young equation [46] of 1805, where  $\sigma_{sv}$  and  $\sigma_{sl}$  are the solid/vapor and solid/liquid interfacial energies, and  $\sigma_{lv}$  is the liquid/vapor interfacial energy (or tension).

<sup>6</sup> Equilibrium situation actually is one single droplet, yet it normally takes too long to reach this state. Before, a network of droplets is formed.

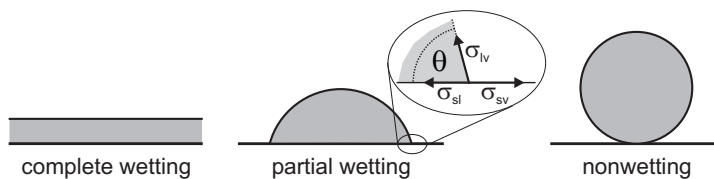


**Fig. 2.** Sketch of a liquid drop atop of a solid substrate. Complete wetting is characterized by a contact angle  $\theta = 0$ , partial wetting by  $0 < \theta < \pi$ , and nonwetting by  $\theta = \pi$  (from left to right)

For  $\theta = 0^\circ$ , i.e.  $\sigma_{sv} - \sigma_{sl} \geq \sigma_{lv}$  the droplet will spread and will completely wet the substrate. For  $0^\circ < \theta < 180^\circ$  one speaks of partial wetting, and for  $\theta = 180^\circ$  of non-wetting. All three cases are sketched in Fig. 2. In case of water (resp. oil), a surface is termed 'hydrophilic' ('oleophilic') if  $0^\circ \leq \theta < 90^\circ$  and 'hydrophobic' ('oleophobic') for  $90^\circ \leq \theta \leq 180^\circ$ <sup>7</sup>. In other words, the contact angle in Young's equation is determined by the free energies of interfaces between semi-infinite media.

This is, however, not the full story. Although a first glance at Fig. 2 suggests that the free energy of a homogeneous film should be written as  $\sigma_{\text{film}} = \sigma_{sl} + \sigma_{lv}$ , this approach neglects possible interactions of the two interfaces (solid/liquid and liquid/vapor) with each other, across the liquid film. Such interactions may come up by virtue of van der Waals forces between the involved materials, which may span several tens of nanometers. In the vicinity of the three phase contact line, the interfaces can thus deviate significantly from a straight intersection at Young's angle (cf. Fig. 3). We will come back to this point later, after having discussed in some detail the long-range forces of a stratified system.

These forces are of similar importance for predicting the stability of a liquid film. Their dependence on film thickness determines not only the linear stability against small perturbations of the free surface, but also the scenario by which the initially uniform film is transformed into its equilibrium state, which consists of droplets of contact angle  $\theta$  on the surface [53, 54, 55]. For example, a droplet of photo resist on a semiconductor may exhibit an equilibrium contact angle  $\theta = 20^\circ$  and therefore wets the surface only partially. What does this mean for a photo resist film that was prepared by a non-equilibrium technique (spin coating) on top of the semiconductor? According to Young's equation, the film is not stable. How will the film decay into droplets and at what speed will this process take place at a given temperature? Will there be time to dry or cure the photo resist before it dewets?

Depending on the thickness of the photo resist, the answers will be different, though Young's contact angle  $\theta$  is always the same! Macroscopic and

<sup>7</sup> It should be noted that non-wetting has never been observed on flat surfaces, although some systems (like, e.g., mercury on glass) come quite close.

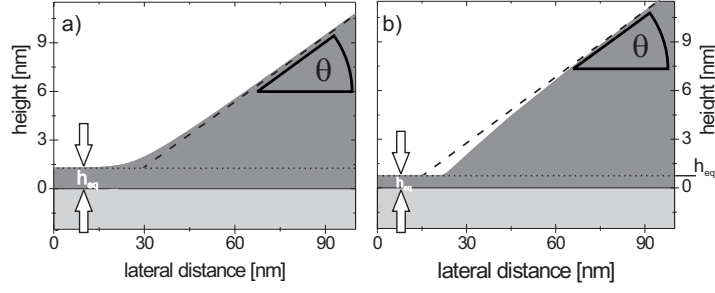


**Fig. 3.** Droplet profiles in the vicinity of the three phase contact line as expected for a) an unstable and b) a metastable situation. The profiles have been calculated for the case of a) a  $d_{SiOx} = 191 \text{ nm}$  on Si and b) a  $d_{SiOx} = 1.7 \text{ nm}$  SiOx layer on Si, the potentials of which are shown in Fig. 7. The dashed line marks the macroscopic contact angle  $\theta = 7.5^\circ$  for a PS drop and the arrows mark the equilibrium wetting layer thickness  $h_{eq}$

molecular terms describing stability conditions often were mixed up and have led to confusion. In what follows, we shall discuss which forces are to be considered, and what typical length scales are involved.

### 3.2 The effective interface potential

Following the preceding section, we *define* the so-called effective interface potential  $\phi(h) \equiv \sigma_{sl} + \sigma_{lv} - \sigma_{film}$ . It comprises both short-range and long-range interactions and is defined as the excess free energy per unit area which is necessary to bring two interfaces from infinity to a certain distance. From its very definition, it is clear that  $\phi(h) \rightarrow 0$  as  $h$  tends to infinity. The excess free energy of an infinitely thick film is thus given by the sum of the free energies of its two interfaces, in accordance with intuition.

For dielectric systems, there are only two relevant types of interactions, steric repulsion and van der Waals forces<sup>8</sup>.

$$\phi(h) = \phi(h)_{steric} + \phi(h)_{vdW} \quad (2)$$

In Fig. 4 three typical curves of  $\phi(h)$  are sketched to illustrate the general principle. Line (1) characterizes a film that is stable on the substrate, since energy would be necessary to thin the film. The equilibrium film thickness is infinite. The two other curves exhibit a global minimum of  $\phi(h)$  at  $h = h_{eq}$ : Curve (2) characterizes a film that is unstable, whereas line (3) describes a metastable film.

<sup>8</sup> A detailed description for numerous different situations involving e.g. polar molecules or hydrogen-bonds or the interactions of a colloidal sphere interacting with a metallic surface can be found in the textbook of J. Israelachvili[48].

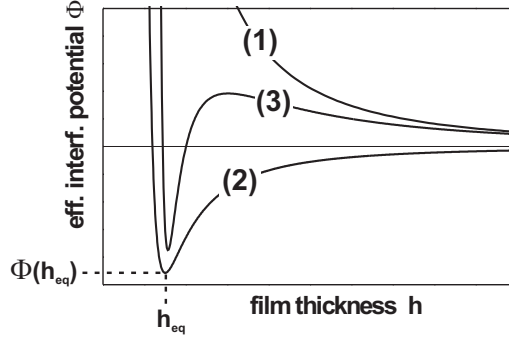


**Fig. 4.** Sketch of the effective interface potential  $\phi$  as a function of film thickness. Line (1) denotes the stable case, line (2) the unstable one and curve (3) the metastable case. The thickness of the stable wetting layer is termed  $h = h_{eq}$ , and is typically in the order of some nm, the depth of the global minimum of  $\phi$  is named  $\phi(h_{eq})$ .

It is readily shown by a linear stability analysis [56, 57, 58] that if the second derivative of  $\phi(h)$  with respect to  $h$  is negative ( $\phi''(h) < 0$ ), unstable modes exist whose amplitudes grow exponentially according to  $\exp(t/\tau)$ , where  $\tau$  is the growth time that is characteristic for the respective mode. Furthermore, there is a characteristic wavelength  $\lambda_s$  of these modes the amplitude of which grows fastest and will therefore dominate the emerging dewetting pattern.

The linear stability analysis also reveals that the spinodal wavelength  $\lambda_s$  is linked to the (second derivative of the) effective interface potential [56, 57]:

$$\lambda_s(h) = \sqrt{\frac{-8\pi^2\sigma_{lv}}{\phi''(h)}}. \quad (3)$$

The spinodal wavelength  $\lambda_s$  is the key to clearly identify a spinodal dewetting process in experimental systems.<sup>9</sup>

One question is now to be answered: What links the effective interface potential to Young's contact angle? The effective interface potential can describe a non-equilibrium situation, yet Young's contact angle is only defined for the equilibrium. A. Frumkin has published in 1938 that[60]

$$\frac{\phi(h_{eq})}{\sigma_{lv}} = \cos \theta - 1. \quad (4)$$

<sup>9</sup> The name 'spinodal dewetting' has been coined due to the analogy to spinodal decomposition of a blend of incompatible liquids, which occurs if the second derivative of the free energy with respect to the composition is negative[59]. As in dewetting, this mechanism is clearly distinct from heterogeneous nucleation, in which randomly distributed impurities dominate the emerging pattern. [13]

What is the consequence of Eq. (3) and Eq. (4)? Determining the spinodal wavelength  $\lambda_s$  as a function of film thickness  $h$  enables us to gain insight into the course of  $\phi''(h)$ . By additionally measuring the equilibrium layer thickness  $h_{eq}$  and the contact angle  $\theta$ , it is possible to reconstruct the complete effective interface potential,[29, 30, 6] c.f. Fig. 7, as will be shown later.

The steric and the van der Waals part of the effective interface potential are characterized by different exponents and different interaction constants, therefore we will discuss the interactions separately:

**Steric repulsion** and chemical interactions are relevant only within a few Ångströms of film thickness, and the resulting force is therefore termed ‘short-range force’. The repulsion is due to overlapping electron shells and is typically described by a higher-order polynomial function and varies as  $1/h^{12}$ , where  $h$  is the distance between the interacting bodies and is difficult to quantify. Considering two planar surfaces, this repulsion yields an interaction energy varying as

$$\phi(h)_{steric} = \frac{C}{h^8}, \quad (5)$$

where  $C$  is a constant characterizing the interaction strength<sup>10</sup>. The reason for the lower exponent in the flat film geometry lies in fact that mutual interaction between all involved atoms or molecules have to be considered. For an extended derivation of the equations we like to refer to J. Israelachvili’s approach<sup>11</sup>.

**Van der Waals interactions** characterize attractive intermolecular forces of quantum-electrodynamic origin. They arise from the variations of the zero-point energies of the collective electromagnetic modes of the system under study. The van der Waals energy between two molecules turns out to vary as  $1/h^6$  in the non-retarded approximation. This approximation holds as long as the lateral dimensions of the system are much smaller than the wavelength of the electromagnetic fields at the dominant excitation energies. Considering retardation effects, the interaction falls off as  $1/h^7$ . In the following, we use only non-retarded potentials since in the experimental systems, effects due to retardation are mostly camouflaged by experimental error bars. Nevertheless, in some special cases including cryogenic systems, retardation effects have been reported [2] and a recent theoretical study [61] discusses their possible influence on thin films in the context of the full theory of Dzyaloshinskii, Lifshitz, and Pitaevskii [62].

Considering again two planar surfaces, the non-retarded interaction yields [48, 63]

$$\phi(h)_{vdW} = -\frac{A}{12\pi h^2}, \quad (6)$$

<sup>10</sup> This definition of  $\phi(h)_{steric}$  here is such that  $C$  is positive and thus the interaction always repulsive.

<sup>11</sup> Here, chapter 10 in the textbook of J. Israelachvili [48] is very helpful.



where  $A$  is the Hamaker constant[64] and  $\phi(h)$  is the energy per unit area. A retarded interaction is described as  $\phi(h) \sim A/h^3$ .

The van der Waals forces of two media interacting through vacuum are always attractive, and  $A$  is positive. If the vacuum yet is replaced by a third medium (e.g. a liquid film), things get more involved: In a system consisting of three media  $m_1/m_3/m_2$ , it may happen that  $m_1$  attracts  $m_2$  stronger than  $m_3$  attracts  $m_2$ . Thus  $m_2$  is 'repelled' by  $m_3$ , this means that the Hamaker constant is negative. To describe the entire system, the Lifshitz theory[65] has to be applied. Here, the interacting bodies are treated as continuous media and the atomic structure is ignored [65, 48, 62]. Rather, bulk properties as the dielectric constants and the refractive indices are used to calculate the Hamaker constant.

For the sake of completeness, we cite here the formula<sup>12</sup> for the Hamaker constants from the book of J. Israelachvili[48], which has proven to be very useful. It is valid for two media 1 and 2, interacting through media 3. All media are taken as being dielectric with a single electronic absorption frequency  $\nu_e$ , which is typically in the range of  $3 \cdot 10^{15}$  Hz;  $n$  is the refractive index of the medium in the visible and  $\epsilon$  the dielectric constant (i.e.  $n_i^2 = \epsilon_i$ , taken in the visible spectral range)

$$A = A_{\nu=0} + A_{\nu>0} \quad (7)$$

$$\approx \frac{3}{4}kT \left( \frac{\epsilon_1 - \epsilon_3}{\epsilon_1 + \epsilon_3} \right) \left( \frac{\epsilon_2 - \epsilon_3}{\epsilon_2 + \epsilon_3} \right) \quad (8)$$

$$+ \frac{3h\nu_e}{8\sqrt{2}} \frac{(n_1^2 - n_3^2)(n_2^2 - n_3^2)}{\sqrt{(n_1^2 + n_3^2)}\sqrt{(n_2^2 + n_3^2)}\{\sqrt{(n_1^2 + n_3^2)} + \sqrt{(n_2^2 + n_3^2)}\}} \quad (9)$$

The Hamaker constant  $A$  will then give the strength of the van der Waals forces between the two interfaces solid/liquid and liquid/air.

For air as medium 1, Si as medium 2 and polystyrene as medium 3, Eq. 9 gives<sup>13</sup>  $A_{Si} = -2.2(5) \cdot 10^{-19}$  J, replacing Si as medium 2 by silicon dioxide, the Hamaker constant is  $A_{SiOx} = 1.8(4) \cdot 10^{-20}$  J. For a silane (OTS) covered Si wafer, the Hamaker constant for the interaction with PS is calculated to be  $A_{OTS} = 1.9(3) \cdot 10^{-20}$  J. For  $A < 0$  ( $A > 0$ ), the system can gain energy by enlarging (reducing) the distance  $h$  between the surfaces, in other words, a polystyrene film of thickness  $h$  is stable on Si, since  $A < 0$ .

In Fig. 5, the dotted line represents the van der Waals potential,  $\phi(h)_{vdW}$ , as given by Eq. 6 for a polystyrene film on a Si wafer, where  $A_{Si}$  is negative. The potential therefore is positive, purely repulsive<sup>14</sup> and the PS film will be

<sup>12</sup> Confer chapter 11, Eq. 11.13 of Ref.[48]

<sup>13</sup> The error of the Hamaker constant is a result of the uncertainties of the optical properties of the involved materials as found in literature. The error for the last digit is given in brackets.

<sup>14</sup> The terms 'attractive' and 'repulsive' can be misleading if thinking of the thin film, yet the terms are chosen for a system of two media (in our case solid and

stable. However,  $\phi(h)_{vdW}$  for PS on an infinitely thick SiOx layer (solid line) is always negative, purely attractive and the PS film will be unstable, since the Hamaker constant  $A_{SiOx}$  is positive.

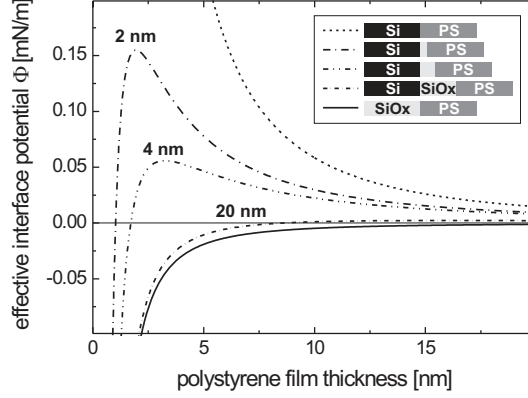


**Fig. 5.** Long-range part of the effective interface potential  $\phi(h)$  as function of PS film thickness  $h$  for different SiOx layer thickness ranging from 0 nm (dotted line) to infinity (solid line), calculated with the formula given in Eq. (10). The Hamaker constants were calculated from the optical constants of the involved materials[48].

Due to the  $1/h^2$  dependence of the potential, the van der Waals forces are long-range forces and act significantly on distances up to about 100 nm. In stratified systems with more than one layer between the two half spaces of media 1 and 2, all mutual interactions have to be considered. The exact calculation of the van der Waals potential may therefore be quite cumbersome. This is an important point, since there is a number of publications that disregard this aspect and claim that theory and experiment do not match. A system like a PS film in air, spun on a thin silicon oxide layer on top of a Si wafer involves two thin layers (three interfaces, abbreviated as air/PS/SiOx/Si) and can be described by two Hamaker constants. So far, no discrepancies between theory and experiment have ever been observed when the formulas given above had been used. One of the most impressive successes is the quite accurate prediction of the critical wetting temperature of pentane on water [66].

Assuming additivity of forces, the system air/PS/SiOx/Si can be characterized by a summation of the van der Waals contributions of each of the single layers with thickness  $h$  of the PS and  $d_{SiOx}$  of the SiOx layer:

---

air) interacting through a third one, here the liquid layer. Hence attractive and repulsive are meant for air being attracted to the solid surface or 'repelled'. In case it is repelled, the effective interface potential is repulsive for the respective thickness of the liquid layer and the liquid wets the solid.

$$\phi_{vdW}(h) = -\frac{A_{SiOx}}{12\pi h^2} + \frac{A_{SiOx} - A_{Si}}{12\pi(h + d_{SiOx})^2}, \quad (10)$$

where  $A_{SiOx}$  and  $A_{Si}$  are the Hamaker constants of the respective system air/PS/SiOx and air/PS/Si. Although not exact,<sup>15</sup> the concept allows to calculate the interaction energies even for stratified systems. With the help of Eqs. (9) and (10), the van der Waals potential of the experimental system is accessible, if the SiOx layer thickness is known and the Hamaker constants are calculated as shown before. Fig. 5 depicts the van der Waals potential as gained from Eq. (10). Clearly, the potential is influenced by the thickness of the silicon dioxide layer.

So the widely used system air/PS/OTS/SiOx/Si can be described by

$$\phi_{vdW}(h) = -\frac{A_{OTS}}{12\pi h^2} + \frac{A_{OTS} - A_{SiOx}}{12\pi(h + d_{OTS})^2} + \frac{A_{SiOx} - A_{Si}}{12\pi(h + d_{SiOx} + d_{OTS})^2}, \quad (11)$$

yet the long-range potential  $\phi_{vdW}$  is not much different to a system with an SiOx layer of thickness  $d_{OTS} + d_{SiOx}$ , since the optical properties of the OTS and the SiOx layer are very similar. The difference in wetting behavior will only be obvious if the short-range potential is added.

To conclude so far,  $\phi(h)$  combines short- **and** long-range interactions. Short-range interactions are difficult to quantify, yet van der Waals interactions can be captured by the optical properties of the involved materials, even for stratified systems, where the suitable van der Waals potential must be taken. If  $\phi''(h) < 0$ , spinodal dewetting is possible and a characteristic wavelength  $\lambda_s$  should be imprinted on the dewetting pattern.

## 4 Experiments: Linking the effective interface potential to macroscopic properties

In this section experimental results shall be compared to the predictions made by the effective interface potential. Typical experimental dewetting patterns in the system air/PS/SiOx/Si are shown in Fig. 6. What can we learn from analyzing the dewetting films? I) By AFM, the contact angle  $\theta$  of droplets in the late stage of dewetting can be measured. II) The equilibrium film thickness  $h_{eq}$  can be determined, e.g. by ellipsometry. III) The spinodal wavelength  $\lambda$

<sup>15</sup> It should be noted here that numerous studies have tried to use only one so-called 'effective Hamaker constant' for stratified systems using combining rules of the form  $A_{132} \approx (\sqrt{A_{22}} - \sqrt{A_{11}})(\sqrt{A_{22}} - \sqrt{A_{33}})$ . However, these rules can only achieve good results under severe limitations, e.g., if the zero-frequency contribution  $A_{\nu=0}$  in Eq. (9) is negligible [48]. Strictly speaking, they are plain wrong, and should be used, if at all, with utmost care. It is not surprising that many of the studies which have used them could not quantitatively reconcile the theoretical description with the experimental results.

and IV) the growth time  $\tau$  of the spinodal pattern can be determined. V) The morphology of the pattern. VI) The growth of the size of the holes and VII) the form of the liquid front as function of time.

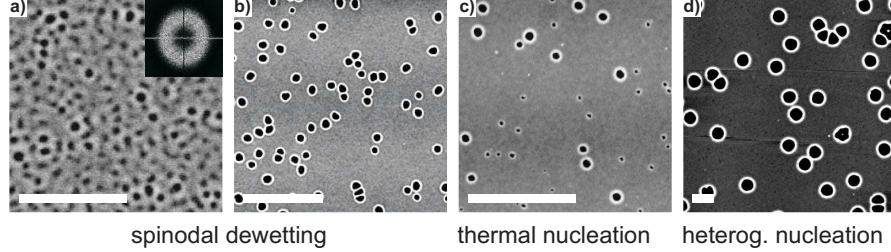


**Fig. 6.** a)-d) AFM images of dewetting PS(2k) films on Si wafers with variable Si dioxide layer and PS film thickness. Scale bars indicate  $5\ \mu\text{m}$ , z-scale ranges from 0 (black) to 20 nm (white): a) 3.9 nm PS film on a Si wafer with  $d_{\text{SiO}_x} = 191\ \text{nm}$ . The inset shows a Fourier transform of the image. b) 3.9(2) nm PS, c) 4.1 nm PS and d) 6.6 nm PS on Si wafers with  $d_{\text{SiO}_x} = 2.4\ \text{nm}$ . (The statistical analysis of the distribution of hole sites in cases (b) to (d) was performed on larger sample areas.)

Dewetting patterns like the one in Fig. 6a clearly exhibit the spinodal wavelength. Fig. 7a comprises experiments with different PS film thicknesses on Si wafers with  $d_{\text{SiO}_x} = 2.4\ \text{nm}$  (open symbols) and with  $d_{\text{SiO}_x} = 191\ \text{nm}$  (filled symbols). From the data of  $\lambda(h)$  data points for  $\phi''(h)$  can be gained. Now, fitting the second derivative of Eq. (10) to the data, the Hamaker constants and the short-range interaction constants can be obtained as fit parameters and the entire effective interface potential can be inferred. It is plotted in Fig. 7b.

The best fits[29, 30] are achieved for  $A_{\text{Si},\text{fit}} = -1.3(6) \cdot 10^{-19}\ \text{J}$  and  $A_{\text{SiO}_x,\text{fit}} = 2.2(4) \cdot 10^{-20}\ \text{J}$ . The values for  $A$  nicely match the values calculated from optical properties of the media involved, as described by Eq. 9. For  $C$  we find  $C_{\text{SiO}_x,\text{fit}} = 6.3(1) \cdot 10^{-76}\ \text{Jm}^6$  and  $C_{\text{OTS},\text{fit}} = 2.1(1) \cdot 10^{-81}\ \text{Jm}^6$ . In the cited references, a detailed description of the fitting and reconstruction procedure can be found.

The second derivative  $\phi''(h)$  is plotted in in Fig. 8a for three SiOx layer thicknesses. An arrow marks the zero in the respective second derivative, corresponding to the relevant inflection points of the curves displayed in Fig. 7b. Spinodal dewetting is possible only for films thinner than indicated by the arrows: PS films on Si wafers with an 1.7 nm (2.4 nm) thick oxide layer are unstable for PS film thicknesses below 3 nm (4 nm). For larger thicknesses, the films are metastable and need to overcome a potential barrier in order to finally reach the global minimum of  $\phi$ . The maximum in  $\phi$ , which is visible in Fig. 7b for the broken curves, represents only part of this barrier, since a nucleus for dewetting as it is formed, e.g., by thermal activation, is a localized

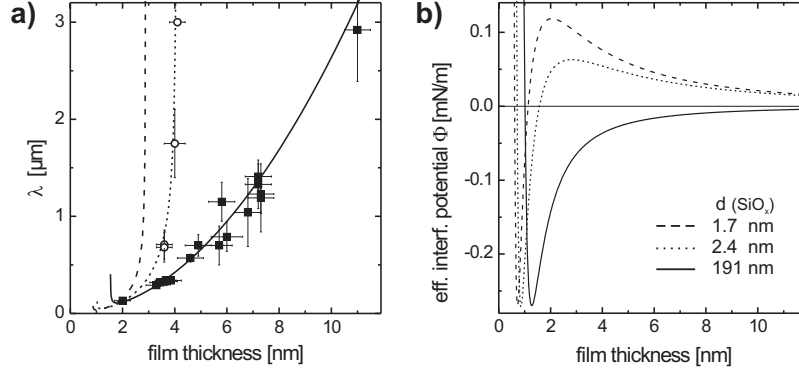


**Fig. 7.** a) Spinodal wavelength as function of PS film thickness on Si wafers with  $d_{\text{SiOx}} = 2.4$  nm (open symbols) and with  $d_{\text{SiOx}} = 191$  nm (filled symbols). b) The effective interface potential  $\phi(h)$  for three different SiOx layer thicknesses.

structure and thus involves excess surface energy as well [68]. It is readily checked that the energy required to form such nucleus is in almost all cases large as compared to  $kT$ , such that thermal nucleation plays no role in systems of practical interest. This can be illustrated nicely with the PS films, as shown in Fig. 8b. PS films on thick 191 nm SiOx (solid line in Fig. 7a) are unstable for all relevant film thicknesses. On 2.4 nm of oxide, however, a sign reversal is observed at a film thickness of about 4 nm (white arrow in Fig. 8a). Only very close to this point, the height of the potential barrier vanishes, and homogeneous nucleation by thermal activation is possible [68, 45, 69]. However, nucleation can as well, and usually does, proceed by means of localized defects in the film. A defect, be it in the molecular texture of a polymeric film or just a small dust particle, may remove the potential barrier locally and thus induce dewetting. This rupture mechanism is termed ‘heterogeneous nucleation’ [59, 67], in analogy to defect-mediated nucleation in demixing scenarios.

The fact that the effective interface potential can be directly inferred from macroscopic quantities, such as the spinodal wavelength, is one reason why experimentalists are seeking for spinodally dewetting regimes in thin liquid film systems. However, if a company is asking why their coating does not stay stable on a surface, it is convenient to rather have a stability diagram which allows to look up where the system will be in a metastable or an unstable state. A stability diagram for the system air/PS/SiOx/Si is shown in Fig. 8b. The solid lines of the diagram base on Eq. 2 with a long-range potential as in Eq. 10 and separate the spinodal dewetting (unstable) regime, where  $\phi''(h) < 0$ , from in the regime of heterogeneous nucleation, characterized by  $\phi''(h) > 0$  (metastable regime). Thermal nucleation is possible for  $\phi''(h) = 0$ , this line separates the two regimes. Experiments that exhibit spinodal dewetting

patterns are indicated by open symbols, those of heterogeneous nucleation (randomly distributed holes) are indicated by solid symbols<sup>16</sup>. A star marks the set of parameters where thermal nucleation was observed. Note that in the unstable regime, heterogeneous nucleation from localized defects is also possible and indeed is sometimes observed. In fact, it usually dominates if the experiments are not performed in extremely clean conditions. Spinodal dewetting, however, can only take place in the unstable regime.

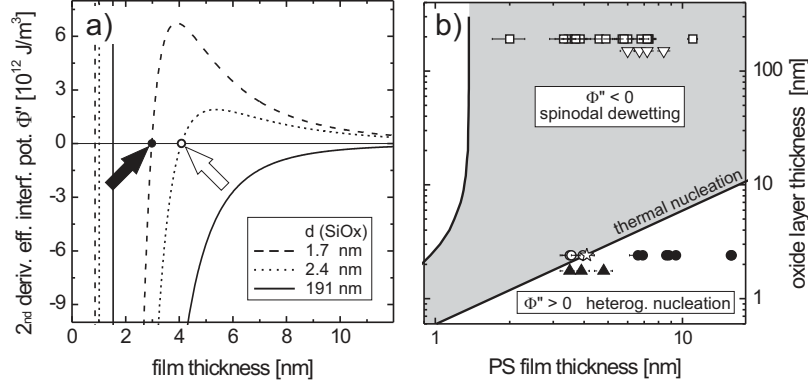


**Fig. 8.** a) Second derivative of the effective interface potential as function of film thickness for three different SiOx layer thicknesses as fitted to the data of Fig. 7. b) Stability diagram of PS films on top of Si wafers with variable oxide layer thickness.[29]

We can state here that the effective interface potential indeed is the key for wetting properties of liquids on surfaces. It can easily be obtained via the optical properties of the involved media and by taking into account the adapted van der Waals potential for stratified systems. It is worth noting that metastable potentials can only be present if there is more than one Hamaker constant involved, one with negative and one with positive sign.

Coming back to the company - a stability diagram for their specific system will reveal the way to a solution of their wettability problem: If their coating system is located in the metastable regime (in the example shown, it depends on the silicon dioxide thickness and the polystyrene thickness), the advice is to reduce the number of possible nucleation centers, e.g. by creating a cleaner environment. If the coating system yet is in the unstable regime, the introduction of an adhesion promoter is necessary.

<sup>16</sup> As explained above, thermal nucleation can be only observed if the nucleation barrier is of order  $kT$ . On the scale of Fig. 8b, this is fulfilled only in a region smaller than the width of the line denoted 'thermal nucleation'. Alleged observations of thermal nucleation in a wider range [70] appear very questionable.

As mentioned at the beginning, the shape of a droplet close to the three phase region is influenced by the long-range intermolecular interactions. By AFM, this region can be characterized. For a detailed discussion we like to refer to the work of T. Pompe et al.[71, 72]. In Fig. 3 two profiles are sketched that were calculated based on the knowledge of the effective interface potential. Fig. 3a is a characteristic curve for an unstable potential as shown for  $d_{SiOx} = 191 \text{ nm}$  in Fig. 7a, whereas a profile like Fig. 3b is expected for a metastable potential like for  $d_{SiOx} = 1.7 \text{ nm}$ . The experimental AFM results (not shown here) corroborate the theoretical expectations[73].

One question is open up to now: are spinodal dewetting patterns always as easy to detect as in Fig. 6a? The answer is 'no': patterns which at first glance appear like the one shown in Fig. 6b can be generated due to a spinodal process as well [6]. The next section we will briefly explain how to distinguish a dewetting pattern of a system in the metastable state from one in the unstable regime and also address thermal nucleation.

## 5 Characterizing experimental dewetting patterns

The three rupture scenarios **spinodal dewetting**, **homogeneous nucleation**, and **heterogeneous nucleation** give rise to specific dewetting patterns. Vice versa, characterizing the experimental dewetting pattern can help to identify the rupture mechanism and to infer the effective interface potential. Fig. 1 and Fig. 6 show experimental examples of films dewetting via different rupture mechanisms. Theoretically, the distinction between nucleation and spinodal dewetting appears quite clear: Vrij [56] proposed already in 1966 that a **spinodal rupture** of a free liquid film results in a dewetting pattern of 'hills and gullies' with a preferred distance  $\lambda_s$  after a certain time of rupture  $\tau$ .

Experimentally, the rupture time  $\tau$  is difficult to measure since the hole which forms as the film has thinned to zero thickness must have a certain size to be observable. Experimentalists thus concentrated instead on the evidence of a preferred wavelength  $\lambda_s$  observable in their systems.<sup>17</sup> If, however, the holes are randomly (Poisson) distributed, they are assumed to stem

<sup>17</sup> Note that a preferred hole distance  $\lambda_s$  has to be distinguished from a mean hole distance: In some studies it was found that the mean hole distance scaled with the film thickness as expected for spinodal dewetting [10, 74]. Therefore, the scenario shown in Fig. 1a was often regarded as a typical spinodal dewetting scenario. However, it turned out later that this was not correct:[13] first of all, the system is metastable for the film thicknesses studied, as an analysis similar to Eq. 10 would have shown. Secondly, the typical time scale for spinodal dewetting does not fit the theoretical expectation (rupture time  $\tau \propto h^5$ ).

from **heterogeneous nucleation**, reflecting the fact that defects typically exhibit random statistics. Although it was generally accepted later that (heterogeneous) nucleation from localized defects is the reason for the dewetting scenario shown in Fig. 1a, the very nature of the nucleation defect mostly remains unclear: it might be dust particles or any other chemical or physical inhomogeneities. In some holes, by light microscopy or atomic force microscopy (AFM), a nanoscopic object could be observed right in the center of each hole. Assuming the object to be a dust particle, the first trial was to reduce the number of nucleation centers by improving the preparation conditions. The number of holes, however, could not be reduced below a certain level, which suggests that the physics of hole nucleation in polymer films may be deeper than a mere effect of ‘dirt’. It has been shown experimentally that stress inside the thin films (stretched entanglements[75]) caused by the preparation of the film out of solution plays a significant role and can cause holes. Details can be found in the studies of Seemann et al.[73] and Reiter et al. [39] .

The experimental distinction between a hole pattern with preferred hole distance and a pattern with randomly distributed hole sites is far from being obvious. The thicker the films are, the weaker is the driving force, and the longer is the growth time  $\tau$  of the spinodal mode[56, 57, 30] (typically,  $\tau \propto h^5$ ) and can easily exceed experimental time scales. For thicker films, dewetting by heterogeneous nucleation may therefore be quicker and can suppress a spinodal pattern [76, 77]. Moreover, chemical heterogeneities can locally cause a change in  $\phi$  and therefore the rupture conditions of the sample may vary from spot to spot leading to a less-ordered dewetting pattern. This effect is more pronounced in thicker films due to the small driving forces and the large growth time  $\tau$ . Hence a two-point correlation function (a radial pair correlation function  $g(r)$  or a Fourier transform) might not be sensitive enough to detect the correlations between the hole sites, or the statistics is too poor. Then, more powerful tools have to be applied. Minkowski functionals - based on integral geometrical methods - have shown to be a versatile method to track down higher order correlations. There is no room here to dwell on this method in any reasonable detail. The reader is referred to the pertinent literature [78, 6, 13, 79, 32, 33].

Let us come back to thermal nucleation once more. As discussed above, the potential barrier for nucleation of a dry spot may in principle be overcome by thermal activation, provided the system is sufficiently close to the sign reversal of  $\phi''(h)$ . The characteristic feature of this scenario is a continuous breakup of more and more holes, whereas nucleation from defects causes holes that emerge only within a sharp time window [28]. Fig. 6c depicts an example for a 4.1 nm thick PS films on a wafer with a 2.4 nm SiOx layer: Holes of different sizes are observable. For that system, the stability diagram of Fig. 8b reads that  $\phi''(4.1 \text{ nm}) \approx 0$ , which is another strong indication that the theoretical predictions corroborate the experimental observations and are able to capture the wettability of dielectric systems.



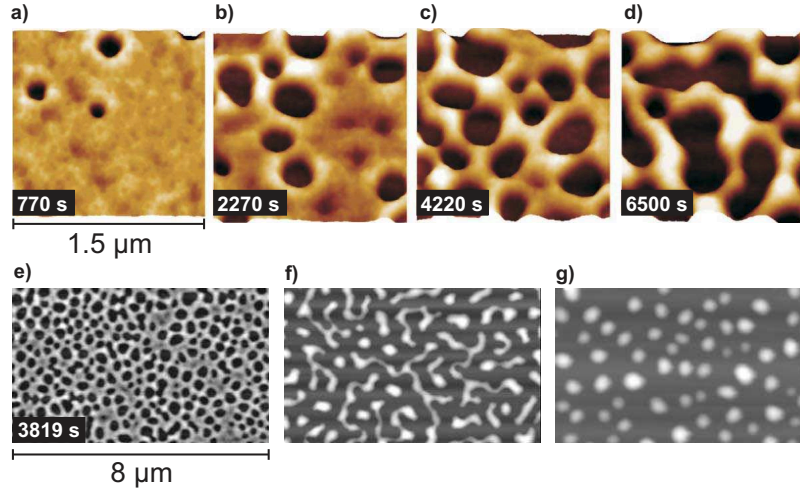


**Fig. 9.** Dewetting morphology of a 3.9(2) nm PS(2k) film on a Si wafer with a 191 nm thick SiOx layer as recorded by in situ AFM. Up to about 5000 s (e) the temperature was held constant at 53° and annealing times are given in the pictures. Afterwards, the temperature was successively increased to 100°. The scan size in (a)(d) is 1.5  $\mu\text{m}$ . In (e)(g) larger scans were made to check possible damage of the sample by the AFM tip. Scan (e) was taken some minutes before scan (d), whereas scan (f) was recorded some minutes after scan (d). Scan (g) characterizes the end of the dewetting process and Ostwald ripening of the droplets slowly sets in.

## 6 Dynamics of spinodal dewetting

At the beginning of spinodal dewetting studies, only one system was known to dewet spinodally: thin gold films on top of quartz substrates [5]. Metal films, however, are not so easy to deal with as compared to polymer films, since the films need to be annealed by a laser. Hence, the time scale is in the ns range, crystallization plays a role and the Hamaker constants are not so easy to calculate. Polymer films such as polystyrene (PS), however, are dielectric and Hamaker constants can easily be determined via Eq. 9.

In situ AFM studies on a dewetting PS film on a Si wafer with a thick SiOx layer reveal the dynamics of the structure formation process, c.f. Fig. 9. Fig. 10 depicts results of Fourier transforms of the AFM scans. Clearly, one mode is amplified fastest. The amplitude of the growing unstable mode, shown in the inset, grows exponentially with time, as expected from theory. Further investigations show that at the onset of the dewetting, no mode is specifically selected, rather, the amplitude reflects the roughness of the film. Comparing the results to deterministic simulations,[32] the pattern formation process and the morphology of the dewetting structures match very well, yet the tempo-

ral evolution of the morphology slightly differs. It turned out that thermal fluctuations accelerate the dewetting dynamics in the experiments.[69, 33]

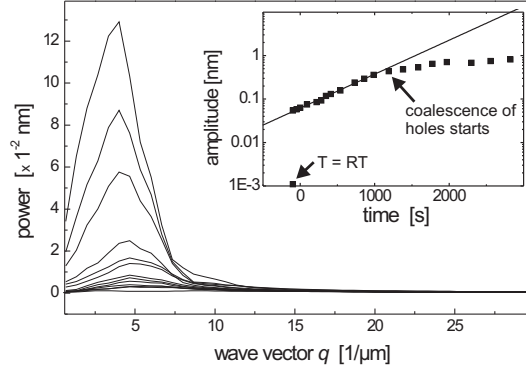


**Fig. 10.** Results of Fourier transforms giving the power spectral density of in situ AFM pictures at  $T = 53^\circ\text{C}$ , one of which is shown in Fig. 6a. Note that the time intervals between the curves are not constant. The inset depicts the amplitude of the undulation as a function of annealing time. The first data point at  $t = 0$  s gives the roughness of the PS film surface at room temperature (RT) as revealed from a Fourier transform. The solid line is a fit of an exponential growth to the data, as expected from theory[57].

## 7 Conclusion

The wettability of a substrate is a delicate interplay of forces. For dielectric systems, the wettability can be described successfully by the effective interface potential  $\phi$ , which is a sum of short- and long-range interactions. The latter are dominated by van der Waals interactions. Their strength can be obtained by calculating the Hamaker constant via the optical properties of the involved media. For stratified systems, the additivity of forces can be assumed.

Rupture mechanism, pattern formation, morphology and dynamics of dewetting are all governed by the effective interface potential and the experiments can corroborate the theoretical expectations.

The knowledge of the effective interface potential therefore allows for a tailoring of the wettability on demand and is a great tool for further fundamental or applied studies.

## References

1. B. Evans and M. Chan, *Physics World* **9**, 48-52, (1996).

2. E. S. Sabisky, C. H. Anderson, Phys. Rev. A **7**, 790-806 (1973).
3. J. E. Rutledge, P. Taborek, Phys. Rev. Lett. **69**, 937-940 (1992).
4. S. Herminghaus et al., Ann. Physik **6**, 425-447 (1997), and references therein.
5. J. Bischof, D. Scherer, S. Herminghaus, and P. Leiderer, Phys. Rev. Lett. **77**, 1536 (1996).
6. S. Herminghaus, K. Jacobs, K. Mecke, J. Bischof, A. Fery, M. Ibn-Elhaj, and S. Schlagowski, Science **282**, 916 (1998).
7. D.G. Bucknall, Progress in Materials Sci. **49**, 713 (2004) and references therein
8. P. Müller-Buschbaum, J. Condens. Matter **15**, R1549 (2003) and references therein
9. C. Redon, F. Brochard-Wyart, and F. Rondelez, Phys. Rev. Lett. **66**, 715 (1991)
10. G. Reiter, Phys. Rev. Lett. **68**, 75 (1992).
11. R. Yerushalmi-Rozen, J. Klein and L. Fetters, Science **236**, 792 (1994)
12. R. Xie, A. Karim, J.F. Douglas, C.C. Han, R.R. Weiss, Phys. Rev. Lett. **81**, 1251 (1998)
13. K. Jacobs, K. Mecke, and S. Herminghaus, Langmuir **14**, 965 (1998).
14. P.G. de Gennes, Rev. Mod. Phys. **57** 827 (1985).
15. P.-G. de Gennes, C. R. Acad. Sci. Paris **B 228**, 219 (1979).
16. R. Seemann, S. Herminghaus, K. Jacobs, Phys. Rev. Lett. **87**, 196101 (2001).
17. R. Fetzer, K. Jacobs, A. Münch, B. Wagner, T. P. Witelski, Phys. Rev. Lett. **95**, 127801 (2005).
18. J. L. Keddie, R. A. L. Jones, R. A. Cory, Europhys. Lett. **27**, 59 (1994).
19. P.-G. de Gennes, Europ. Phys. J. E **2**, 201 (2000) and C. R. Acad. Sci. **1/IV**, 1179 (2000)
20. J. A. Forrest, K. Dalnoki-Veress, Adv. Colloid. Interface Sci. **94**, 167 (2001) and references therein.
21. S. Herminghaus, K. Jacobs and R. Seemann, Eur. Phys. J. E **5**, 531 (2001).
22. S. Herminghaus, K. Landfester, and R. Seemann, Phys. Rev. Lett. **93**, 017801 (2004)
23. J. Baschnagel and F. Varnik, J. Phys.: Condens. Mater. **17** R851 (2005) and references therein.
24. M. Alcoutlabi and G. B. McKenna, J. Phys.: Condens. Mater. **17** R561 (2005) and references therein.
25. S. R. Wassermann, Y. Tao, and G. M. Whitesides, Langmuir **5**, 1075 (1989).
26. J. B. Brzoska, I. Ben Azouz, and F. Rondelez, Langmuir **10**, 4367 (1994).
27. F. Brochard, J.-M. di Meglio, and D. Quéré, C. R. Acad. Sci II **304** 553 (1987).
28. K. Jacobs, R. Seemann, G. Schatz, and S. Herminghaus, Langmuir **14**, 4961 (1998).
29. R. Seemann, S. Herminghaus and K. Jacobs, Phys. Rev. Lett. **86**, 5534 (2001).
30. R. Seemann, S. Herminghaus and K. Jacobs, J. Phys.: Cond. Mat. **13**, 4925 (2001).
31. R. M. A. Azzam, N. M. Bashara, *Ellipsometry and Polarized Light* (Elsevier, Amsterdam 1977).
32. J. Becker, G. Grün, R. Seemann, H. Mantz, K. Jacobs, K. R. Mecke, R. Blossey, Nature Materials **2**, 59 (2003).
33. R. Fetzer, M. Rauscher, S. Seemann, K. Jacobs, and K. Mecke, Phys. Rev. Lett. **99**, 114503 (2007)
34. C. Redon, J. B. Brzoska, and F. Brochard-Wyart, Macromolecules **27**, 468 (1994).
35. F. Brochard, P. G. de Gennes, H. Hervet, C. Redon, Langmuir **10**, 1566 (1994).

36. F. Brochard, C. Redon, C. Sykes, C. R. Acad. Sci II **314**, 19 (1992).
37. G. Reiter, P. Auroy, and L. Auvray, *Macromolecules* **29**, 2150 (1996)
38. G. Reiter and R. Khanna, *Langmuir* **16**, 6351 (2000).
39. G. Reiter, M. Hamieh, P. Dammann, S. Slavons, S. Gabriele, T. Vilmin, and E. Raphael, *Nature Materials* **4**, 754 (2005)
40. R. Fetzer and K. Jacobs, *Langmuir* **23**, 11617 (2007).
41. R. Fetzer, M. Rauscher, A. Münch, B. Wagner, and K. Jacobs, *Europhys. Lett.* **75**, 638 (2006).
42. R. Fetzer, A. Münch, B. Wagner, M. Rauscher, and K. Jacobs, *Langmuir* **23**, 10559 (2007).
43. Lord Rayleigh, F. R. S., *Proc. London Math. Soc.* **10**, 4 (1878).
44. W. Ostwald, 'Lehrbuch der Allgemeinen Chemie', vol. 2, part 1. Leipzig, Germany (1896).
45. S. Herminghaus, F. Brochard, C. R. Physique, **7**, 1073-1081 (2006); see also C. R. Physique **8**, 86 (2007).
46. T. Young, *Phil. Trans. Royal Soc. part I*, 65 (1805).
47. S. Safran, *Statistical Thermodynamics of Surfaces, Interfaces, And Membranes*, (Addison-Wesley Publishing Company: New York, 1994).
48. J. Israelachvili, *Intermolecular Surface Forces* (Academic Press Inc.: New York, 1992), 2nd ed.
49. M. Schick in *Liquids at Interfaces*, J. Charvolin *et al*, Eds (Elsevier Science: Amsterdam, 1989).
50. S. Dietrich in *Phase Transition and Critical Phenomena*, C. Domb and J. L. Lebowitz, Eds (Academic Press: London, 1988) Vol. 12.
51. A. Oron, S. H. Davis, and S. G. Bankoff, *Rev. Mod. Phys.* **69**, 931 (1997).
52. A. Oron, *Phys. Rev. Lett.* **85**, 2108 (2000).
53. R. Seemann, R. Blossey, and K. Jacobs, *J. Phys.: Condens. Matter* **13** 4915 (2001).
54. A. Sharma and R. Khanna, *Phys. Rev. Lett.* **81**, 3463 (1998), and A. Sharma and R. Khanna, *J. Chem. Phys.* **110**, 4929 (1999).
55. D. Quéré, *Nature Materials* **3**, 79 (2004).
56. A. Vrij, *Disc. Faraday Soc.* **42**, 23 (1966).
57. E. Ruckenstein and R. K. Jain, *J. Chem. Soc. Faraday Trans. II* **70**, 132 (1974).
58. M. B. Williams and S. H. Davis, *J. Colloid Interface Sci.* **90**, 1 (1982).
59. V. S. Mitlin, *J. Colloid Interface Sci.* **156**, 491 (1993).
60. A. N. Frumkin, *J. Phys. Chem. USSR* **12**, 337 (1938).
61. H. Zhao, Y. J. Wang and O.K.C. Tsui, *Langmuir* **21**, 5817 (2005).
62. I. E. Dzyaloshinskii, E. M. Lifshitz, and L. P. Pitaevskii, *Adv. Phys.* **10**, 165 (1961).
63. A. W. Adamson, *Physical Chemistry of Surfaces*, J. Wiley & Sons, Inc., New York, 1990.
64. H. C. Hamaker, *Physica* **4**, 1058 (1937).
65. E. M. Lifshitz, *Soviet Phys. JETP (Engl. Transl.)* **2**, 73 (1956).
66. K. Ragil *et al.*, *Phys. Rev. Lett.* **77**, 1532-1535 (1996).
67. V. S. Mitlin, *Colloid Surf. A* **89**, 97 (1994).
68. R. Blossey, *Int. J. Mod. Phys. B* **9**, 3489 (1995).
69. Y.-J. Wang, O.K.C. Tsui, *J. Non-Crystalline Solids* **352**, 4977 (2006).
70. J. P. DeSilva, M. Geoghegan, A.M. Higgins, G. Krausch, M.-O. David and G. Reiter, *Phys. Rev. Lett.* **98**, 267802 (2007).

71. T. Pompe and S. Herminghaus, Phys. Rev. Lett. **85**, 1930 (2000).
72. T. Pompe, Phys. Rev. Lett. **89**, 076102 (2002).
73. R. Seemann, S. Herminghaus, C. Neto, S. Schlagowski, D. Podzimek, R. Konrad, H. Mantz, and K. Jacobs, J. Phys.: Condens. Matter **17**, S267 (2005).
74. G. Reiter, Langmuir **9**, 1344 (1993).
75. S. G. Croll, J. Appl. Polymer Sci. **23**, 847 (1979).
76. R. Konnur, K. Kargupta, and A. Sharma, Phys. Rev. Lett. **84**, 931 (2000), and references therein.
77. C. Neto, K. Jacobs, R. Seemann, R. Blossey, J. Becker, G. Grün, J. Phys.: Condens. Matter **15**, 3355 (2003) and **15**, S421 (2003).
78. K. R. Mecke, *Integralgeometrie in der Statistischen Physik - Perkolation, komplexe Flüssigkeiten und die Struktur des Universums, Reihe Physik Bd. 25* (Verlag Harri Deutsch, Frankfurt a.M., 1994).
79. K. Jacobs, R. Seemann and K. Mecke in *Statistical Physics and Spatial Statistics*, K. Mecke and D. Stoyan, Eds. (Springer: Heidelberg 2000).